The field line map approach for simulations of edge/SOL in divertor geometry

A. Stegmeir[1], D. Coster[1], A. Ross[1], O. Maj[1], K. Lackner[1]

[1] *Max-Planck-Institut für Plasmaphysik, 85748 Garching, Germany*

Field line map approach

Field/flux aligned coordinates are routinely employed in codes for magnetic fusion to exploit the anisotropy of the plasma ($k_{\|} \ll k_{\perp}$). However, due to the fact of being singular on the separatrix/X-point(s) the region of closed magnetic flux surfaces, i.e. the edge, and the region of open field lines, i.e. the scrape-off layer (SOL), cannot be treated on the same footing with field aligned coordinates. The flux-coordinate independent approach (FCI) offers a promising solution in order to deal with a separatrix and X-point(s) in diverted tokamaks [1, 2, 3]. A cylindrical grid, which is Cartesian within poloidal planes, is employed, where discretisation of perpendicular operators is straight forward. The strong anisotropy of the plasma is exploited computationally by coarsening the grid in the toroidal direction and discretising parallel operators via a field line map: For each grid point corresponding map points in the adjacent poloidal planes are computed via tracing along magnetic field lines. With this information discrete versions of parallel operators can be constructed based on finite differences along magnetic field lines. An interpolation is required since the map points do in general not coincide with grid points, and therefore numerical perpendicular diffusion/pollution becomes a very important issue within the FCI approach. Based on the method of support operators a numerical scheme was derived for the parallel diffusion which exhibits a highly reduced level of numerical diffusion as compared to a naive discretisation [3, 4]. Further numerical subtleties, i.e. distortion of the field line map and the treatment of boundaries are discussed in [5]. Besides several codes [2, 3, 6, 7] the FCI is used in GRILLIX. In this paper we concentrate on the effect of geometry on the propagation of blobs.

Phyiscal model

Drift reduced Braginskii equations [8] with cold ions, isothermal electrons and neglect of electron inertia, magnetic induction and parallel ion streaming are employed. The latter assumption is justified if the radial propagation of the blob is dominant over its parallel propagation. The system is then described by the continuity equation and the quasi-neutrality condition,

which are coupled by Ohm's law. In normalized form the equations are:

$$\frac{\partial}{\partial t}n + \frac{1}{B}\frac{R_0}{\rho_{s0}}[\phi, n] = C(n) - nC(\phi) + \nabla\cdot\left(J_\parallel \mathbf{b}\right) + \nu_n \nabla_\perp^6 n \tag{1}$$

$$\frac{1}{B^2}\left\{\frac{\partial}{\partial t}\Omega + \frac{1}{B}\frac{R_0}{\rho_{s0}}[\phi, \Omega]\right\} = C(n) + \nabla\cdot\left(J_\parallel \mathbf{b}\right) + \nu_v \nabla_\perp^6 \Omega, \tag{2}$$

$$J_\parallel = \sigma\nabla_\parallel\left(\log n - \phi\right), \tag{3}$$

with the vorticity $\Omega := \nabla_\perp^2\phi$ in Boussinesq approximation. For description of normalisation we denote dimensional quantities with subscript p in the following. Plasma density $n_p = n_0 n$ with n_0 a reference density; electrostatic potential $\phi_p = \phi T_e/e$; parallel current $J_{\parallel p} = c_s e n_0 J_\parallel$; magnetic field $\mathbf{B}_p = B_0\mathbf{B}$ with B_0 the magnetic field strength on axis; perpendicular coordinates $\mathbf{x}_{\perp p} = \mathbf{x}_\perp \rho_{s0}$ with $\rho_{s0} := \sqrt{T_e M_i}/(eB_0)$; parallel coordinate $x_{\parallel p} = x_\parallel R_0$ with major radius R_0; time $t_p = t R_0/c_s$. The bracket $[\phi, f] := \partial_R\phi\partial_Z f - \partial_Z\phi\partial_R f$ represents E cross B advection and $C(f) := -2\partial_Z f$ is the curvature operator. The high order diffusion terms with coefficients ν_n and ν_v model perpendicular dissipation. The dimensionless parallel conductivity is defined as $\sigma_\parallel := 1.96\frac{c_s/R_0}{\nu_{ei}}\frac{M_i}{m_e}$ with ν_{ei} the electron-ion collision frequency. Linearized sheath boundary conditions $J_\parallel\big|_b = \pm n\phi|_b$ are applied at the target plates [9]. Finally, eqs. (1)-(3) constitute a very basic model and many approximations might certainly be questionable, but due to its simplicity it is well suited for the aim of this work, which is the investigation of effects of the geometry on blob propagation.

Estimations for scaling laws for the radial blob velocity v_b can be obtained from a closure for the parallel current [10]. An important parameter is thereby the blob width δ_b as it controls the relative magnitude of the different terms. A critical blob size of $\delta_* = \rho_s\left(L_\parallel^2/\rho_s R_0\right)^{1/5}$ is found from a sheath current closure, where for blobs of $\delta_b \ll \delta_*$ the sheath current term can be neglected against the inertial term. In this inertial regime the blobs develop the characteristic mushroom-like shape and the blob velocity scales like $v_b \propto \sqrt{\delta_b}$. On the other hand for large blobs of $\delta_b \gg \delta_*$ the inertial term can be neglected yielding as scaling $v_b \propto \delta_b^{-2}$ (sheath limited regime). Blobs are found to propagate most stable at an intermediate scale $\delta_b \approx \delta_*$.

Blob propagation in three geometries

We investigate the propagation of a blob in slab geometry, circular geometry with limiter and in diverted geometry. The diverted geometry [11] (see fig. 1), resembling roughly ASDEX Upgrade, has a connection length from outboard midplane to the outer target of $L_c \sim 4.5R_0$. In the circular geometry the limiter is put at the bottom and the safety factor is chosen such that the connection length from outboard midplane to the outer limiter plate is similar to the connection length in diverted geometry. The slab geometry shall model a flux tube

ranging from the outer target to the inner target, and its axial length (along the magnetic field line) is chosen correspondingly. However, due to technical reasons there is yet no dependence of the curvature on the axial coordinate. The initial state is a ballooning structure with perpendicular Gaussian width of δ_b and a Gaussian parallel structure of $L_\parallel \sim 5R_0$ according to the magnetic geometry with its fanning. The maximum amplitude of the blob exceeds the background by 100%. We consider a deuterium plasma with flat background density of $n_0 = 1 \cdot 10^{19} m^{-3}$ and other parameters as following: $R_0 = 1.65m$, $T_e = 7eV$, $B_0 = 1.5T$, $\nu_{ei} = 1.75 \cdot 10^7 s^{-1}$, which results in $\rho_{s0} = 2.5 \cdot 10^{-4} m$, $c_s = 1.8 \cdot 10^4 ms^{-1}$ and $\delta_* \sim 10\rho_s$.

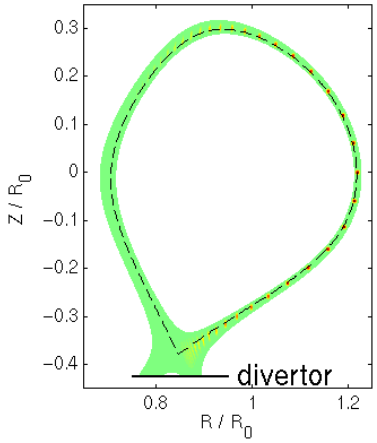

Figure 1: *Diverted geometry with initial state shown superimposed (32 poloidal planes). Dashed line indicates separatrix.*

A snapshot of the density contour of a blob with initial width $\delta_b = 10\rho_{s0}$ is shown in fig. 2 for the three different geometries. 32 poloidal planes with a perpendicular grid resolution of $\Delta x_\perp = \rho_{s0}$ were used and a dissipation acting on the grid scale with $\nu_n = \nu_v = 3.0$ was employed. The overall radial displacement in all three cases is similar. The blob shape is very similar for slab and circular geometry, where the characteristic mushroom shape emerges, whereas in the diverted case the blob appears to be more coherent and exhibit less poloidal drift.

Finally, we scan the radial blob velocity against its initial blob width δ_b. In slab and circular geometry we perform this scan by adapting the perpendicular resolution to the blob width according to $\Delta x_\perp = \delta_b/10$ without applying dissipation. However, this approach might not be justified in diverted geometry where the blob becomes strongly distorted due to magnetic fanning. Hence, in diverted geometry a blob encompasses many perpendicular scales and perpendicular dissipation should be present damping structures falling below the resolution threshold. Therefore, in diverted geometry we fix the perpendicular resolution to $\Delta x_\perp = \rho_{s0}$ and the dissipation to $\nu_n = \nu_v = 3.0$. Due to computational costs a scan over a large range of δ_b in diverted geometry was not possible.

In figure 3a the temporal development of the radial velocity of the center of mass of the blob at outboard midplane is shown for various sizes δ_b in the three different geometries. Small blobs $\delta_b \ll \delta_*$ (inertial regime) decay quickly after having achieved their maximum velocity, whereas large blobs $\delta_b \gg \delta_*$ propagate slowly. Only blobs of size $\delta_b \sim \delta_*$ remain rather stable and therefore propagate a larger radial distance. Overall there is not a strong dependence on the radial propagation velocity on geometry. In fig. 3b the maximum radial blob velocity is plotted against their initial width. Small blobs exhibit the inertial scaling $v_b \propto \sqrt{\delta_b}$ and large blobs

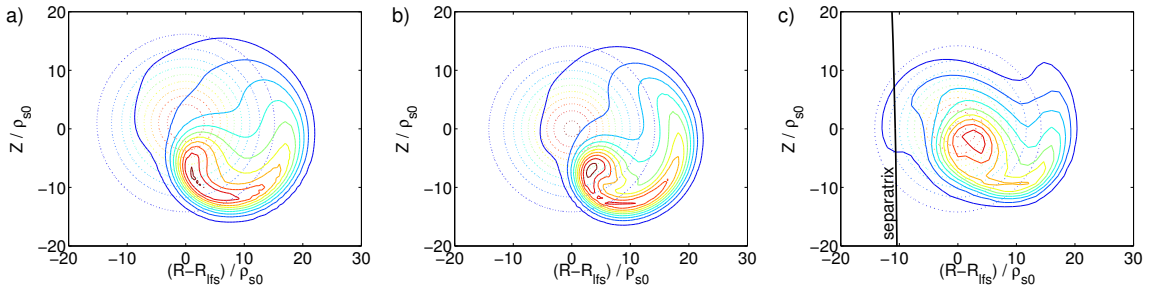

Figure 2: *Contours of density of blob with* $\delta_b = 10\rho_{s0} \sim \delta_*$ *at* $t = 0$ *(dashed) and* $t = 0.18$ *(solid) at outer midplane. a) Slab geometry, b) circular limiter geometry, c) diverted geometry.*

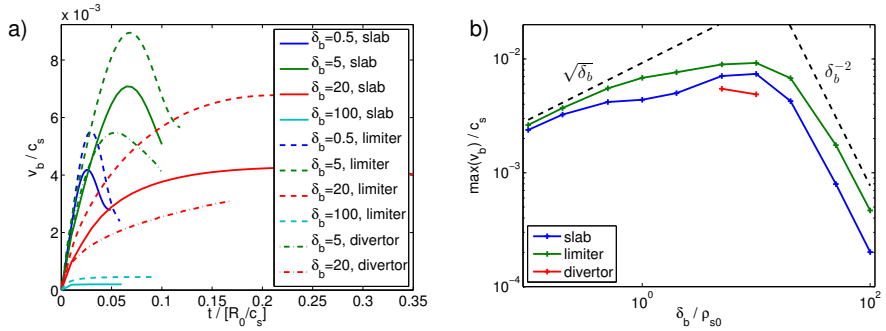

Figure 3: *a) Temporal evolution of radial velocity of center of mass of blob for widths* $\delta_b = 0.5$ *(blue),* $\delta_b = 5$ *(green),* $\delta_b = 20$ *(red) and* $\delta_b = 100$ *(cyan) in slab (solid), circular limiter (dashed) and diverted (dashed-dotted) geometry. b) Maximum radial velocity of center of mass versus* δ_b*. Black dashed lines indicate inertial scaling* ($\propto \sqrt{\delta_b}$) *and sheath limited scaling* ($\propto \delta_b^{-2}$).

the sheath limited scaling $v_b \propto \delta_b^{-2}$, where the transition occurs roughly at $\delta_b = \delta_* \sim 10\rho_{s0}$, in agreement to theory.

A part of this work was carried out using the HELIOS supercomputer system at Computational Simulation Centre of International Fusion Energy Research Centre (IFERC-CSC), Aomori, Japan, under the Broader Approach collaboration between Euratom and Japan, implemented by Fusion for Energy and JAEA. This work has been carried out within the framework of the EUROfusion Consortium and has received funding from the Euratom research and training programme 2014-2018 under grant agreement No 633053. The views and opinions expressed herein do not necessarily reflect those of the European Commission.

References

[1] M. Ottaviani, Phys. Lett. A **375**, 1677 (2011).
[2] F. Hariri and M. Ottaviani, Comput. Phys. Commun. **184**, 2419 (2013).
[3] A. Stegmeir, et al., Comput. Phys. Commun. **198**, 139 (2016).
[4] A. Stegmeir, et al, Contrib. Plasm. Phys. **54**, 549 (2014).
[5] A. Stegmeir, et al., submitted to Comput. Phys. Commun. (2016).
[6] M. Held, et al., Comput. Phys. Commun. **199**, 29 (2016).
[7] B.D. Dudson, et al., arXiv:1602.06747 (2016).
[8] A. Zeiler, et al., Phys. Plasmas, **4**,2134 (1997).
[9] P.C. Stangeby, *The Plasma Boundary of Magnetic Fusion devices*, IOP (2000).
[10] S.I. Krasheninnikov et al., J. Plasma Physics, **74**, 679 (2008).
[11] P.J.M. Carthy, Phys. Plasmas, **6**, 3554 (1999).